Chlorine Partitioning Between a Basaltic Melt and H2O-CO2 Fluids at Mount Etna

Marina Alletti, Don R. Baker, Bruno Scaillet, A. Aiuppa, R. Moretti, L. Ottolini

HAL Id: insu-00376481

https://insu.hal.science/insu-00376481

Submitted on 22 Apr 2009

CHLORINE PARTITIONING BETWEEN A BASALTIC MELT AND H_2O-CO_2 FLUIDS AT MOUNT ETNA

Alletti M.[$,1,3], Baker D.R.[2], Scaillet B.[3], Aiuppa A.[1], Moretti R.[4], Ottolini L.[5]

[1]CFTA, University of Palermo, Via Archirafi,36, Palermo, 90123 Italy

[2]EPS, McGill University, 3450 rue Univeristy, Montreal, QC H3A 2A7

[3] Université d'Orléans, CNRS/INSU, Université François Rabelais - Tours

Institut des Sciences de la Terre d'Orléans - UMR 6113 Campus Géosciences

1A, rue de la Férollerie 45071 Orléans cedex 2 France

[4]INGV-Napoli 'Osservatorio Vesuviano', Via Diocleziano 328, Napoli, 80124 Italy

[5]CNR-Istituto di Geoscienze e Georisorse-Sezione di Pavia, Via Ferrata 1, Pavia, 27100 Italy

[$] Corresponding author:

e-mail: marina.alletti@tin.it

tel: +33 (0)238 25 52 53

fax: +33 (0)238 63 64 88

Abstract

Partitioning experiments between a basaltic melt from Mt. Etna and a low-density hydrous fluid or vapor containing H_2O or H_2O-CO_2 were performed at 1200-1260 °C, at pressures between 1 and 200 MPa, either near the nickel-nickel oxide (NNO) buffer or at two log units above it (NNO+2), and with different chloride concentrations. Most of the experiments were done at chloride-brine-undersaturated conditions, although at the highest Cl concentrations explored brine saturation might have been reached. The average partition coefficients ($D_{Cl}^{fluid/melt}$) over the range of Cl concentrations were derived on a weight basis by plotting the calculated concentrations of Cl in the fluid phase versus the measured ones in the melt. For H_2O-Cl experiments in which the Cl concentration in the melt was ≤ 0.4 wt.%, a negative dependence between $D_{Cl}^{f/m}$ and pressure is observed. $D_{Cl}^{fluid/melt}$ in H_2O+Cl-bearing experiments ranges between 11-14 at 1 and 25 MPa to 6 at 200 MPa at NNO; and between 4 at 50 MPa and 13 at 100 MPa at ΔNNO≥2. Addition of CO_2 at NNO yields lower partition coefficients than in CO_2-free conditions over the pressure range investigated. The negative pressure dependence observed for H_2O-Cl experiments disappears when CO_2 is present in the system. Overall, once CO_2 is introduced in the system, Cl fugacity in the silicate melt tends to increase, thus resulting in a decrease of $D_{Cl}^{f/m}$. Application to Mt. Etna shows that the composition of the volcanic plume in terms of Cl records very shallow pressures of magma equilibration with its exsolved fluid.

1. Introduction

An improved knowledge of volatile solubility and partitioning behaviors between silicate melts and a fluid phase is of great importance for the comprehension of melt properties and the degassing behavior of magmas. Even though halogens (i.e., Cl and F) are only minor components (after H_2O, CO_2 and S) in volcanic gases (Symonds et al., 1994) and in most magmas (Carroll & Webster, 1994; Aiuppa et al., 2009, this issue), they have been shown to affect the physical properties of silicate melts (Wyllie & Tuttle, 1961; Dingwell & Mysen, 1985; Lange, 1994; Giordano et al., 2004; Zimova & Webb, 2007), phase relations (Manning, 1981; Dolejs & Baker, 2004), and to contribute to ore-deposit formation by transporting metals in the hydrothermal environment (Burnham, 1979; Boudreau et al., 1986; Heinrich, 2005). No less important, since halogens are involved in magma degassing, their concentrations are systematically measured in volcanic gases and plumes to interpret and possibly predict the evolution of active volcanoes (Aiuppa, 2009, this issue).

A quantitative understanding of the role played by halogens in volcanic-hydrothermal processes requires knowledge of their solubility in silicate melts, and their vapor-melt partitioning behavior during volcanic degassing. Previous studies have focused on the determination of Cl solubility and partitioning in some highly silicic to intermediate magmas (e.g., Shinohara et al., 1989; Métrich & Rutherford, 1992; Signorelli & Carroll, 2000, 2002; Webster & De Vivo, 2002; Botcharnikov et al., 2004; Webster et al., 2009, this issue), while very few comparable studies have been carried out on low silica melts, i.e., basaltic and andesitic (Iwasaki & Katsura, 1967; Malinin et al., 1989; Webster et al., 1999; Mathez & Webster, 2005; Botcharnikov et al., 2007; Stelling et al., 2008; Chevychelov et al., 2008).

A characterization of halogen behavior in magmas is particularly needed at Mt. Etna, the most active volcano in Europe, which recurrently emits basaltic lavas (Bonaccorso et al., 2004), and whose minerals contain primitive melt inclusions with up to $0.2 - 0.3$ wt.% dissolved chlorine

(Métrich et al., 2004; Spilliaert et al., 2006b). Etna is also characterized by massive halogen degassing from its persistently open summit vents (Pennisi & Le-Cloarec, 1998; Francis et al., 1998), and chlorine and fluorine abundances in the passive and eruptive plumes of Mt. Etna are now routinely measured by either spectroscopic (FTIR) or chemical (filter packs) methods to monitor its volcanic activity (see Aiuppa, 2009, this issue, for a review). Studies of Mt. Etna volcanic gas compositions (Aiuppa et al., 2004; Allard et al., 2005), combined with the application of thermodynamic models for the C-H-O-S system (Moretti et al., 2003; Burgisser & Scaillet, 2007) and melt-inclusion investigations (Spilliaert et., 2006a, 2006b), have emphasized their potential for eruption forecasting (Aiuppa et al., 2007). However, in order to extend such models to halogens, experiments on halogen partitioning between a basaltic melt and a coexisting fluid phase are required. Few experimental data are available, mainly performed at 200 MPa (Webster et al., 1999; Mathez & Webster, 2005; Botcharnikov et al., 2007; Stelling et al., 2008; Chevychelov et al., 2008), and thus we still need constraints at lower pressures relevant to degassing during magma ascent. In this context, our study mainly aims at investigating the distribution of chlorine between a basaltic melt and a coexisting aqueous fluid phase (or phases) at different pressures and redox conditions for H_2O-Cl and H_2O-CO_2-Cl fluids.

In order to reproduce conditions typical of the shallow plumbing system of Mt. Etna (Métrich & Clocchiatti, 1996; De Gori et al., 2005), experiments were performed at log f_{O2} near the nickel-nickel oxide buffer (NNO), at T = 1200 and 1260 °C, for a pressure range of 1 – 200 MPa, and either in presence of a binary (H_2O-Cl) or ternary (H_2O-CO_2-Cl) fluid phase. We also performed experiments at log f_{O2} of ΔNNO$\geq$2, T = 1200 °C and P = 50 and 100 MPa to investigate possible effects of differing redox conditions.

The results of experimental studies, combined with the recently derived melt-inclusion record of degassing paths (Spilliaert et al., 2006a and 2006b), and with measurements of volcanic plumes' compositions at Etna (Aiuppa et al., 2002, 2004), can significantly contribute to our understanding of chlorine behavior in basaltic magmas.

2. Experimental and analytical techniques

2.1 Starting material

A hawaiitic basalt from the Mt. Etna eruption of 2001 (Pompilio 2001) was used as the starting material for the partitioning experiments. The sample was first crushed and ground, then fused in a platinum crucible in a 1-atm furnace at 1400 °C, for 3 hours, in order to melt crystals and remove any H_2O and CO_2 naturally present. The melt was quenched by using a water bath and the resulting glass was then finely ground and stored in a drying oven before use. A small chip of this glass was mounted in epoxy and checked for homogeneity by electron-microprobe analysis (Table 1).

2.2 Experimental methods

2.2.1 1 MPa experiments

The experiments at 1 MPa were performed at McGill University in Montreal, Canada, with a custom-built low-pressure-vertically-operating autoclave constructed from a 0.1 MPa $MoSi_2$ furnace, into which an Al_2O_3 tube was inserted, sealed with aluminum end caps designed to hold 5 MPa (Alletti et al. 2006). This pressure vessel was initially pressurized with argon up to 0.62 MPa, sealed, and heated to 1260±5 °C upon which the experimental pressure of 1 MPa was reached. Temperature was measured by a type S ($Pt – PtRh_{10}$) thermocouple placed next to the sample in the furnace. The thermocouple was calibrated against the melting points of gold and diopside and is accurate to within 2 °C. The thermal gradient in the furnace was measured and during routine operation was less than 5 °C along the length of the capsules used in our experiments. The sample, loaded inside a Pt capsule (see below) and placed inside a Pt wire basket, was hung near the hot spot of the furnace from a thin Pt ($\varnothing = 0.005$ mm) wire.

Two different approaches were used for Cl partitioning experiments at 1 MPa:

1) Chlorine-out experiments: the glass was initially loaded with 0.3 and 0.7 wt.% chlorine as NaCl + ~ 3 wt.% H_2O and melted at 1 GPa and 1300 °C using a piston-cylinder apparatus for 2 hours. Chips of this starting material were then placed in an $Au_{80}Pd_{20}$ tube (Ø = 2 mm), crimped and inserted into a Pt tube (Ø = 10 mm; 12 cm length) and welded.

2) Chlorine-in experiments: the volatile-free glass was initially finely ground and packed in a $Au_{80}Pd_{20}$ tube, crimped and inserted in a Pt tube crimped and welded shut. In the space between the two capsules, we introduced the fluid phase consisting in: 1) 4-5 wt.% of a saline solution (containing either 1.5 wt.% or 4.7 wt.% chlorine, added as reagent NaCl) ; or 2) 3.6 wt.% H2O and either 1.6 or 2.3 wt.% Cl (as reagent NaCl).

We also performed a single experiment at 1 MPa, 1260 °C, for 8 hours in which we added ~ 5000 ppm sulfur (as FeS powder) to the Etna basalt, in order to estimate the intrinsic redox conditions of the autoclave by using the S^{6+}/S_{TOTAL} ratio of the S dissolved in the glass (see section 2.6).

2.2.2 *25 to 200 MPa experiments*

The experiments at 25 to 200 MPa were performed in the laboratory of the ISTO-CNRS University of Orléans, France, using rapid-quench Internally Heated Pressure Vessels (IHPV), operating vertically and pressurized either with Ar or with an Ar-H_2 mixture (see Di Carlo et al., 2006 and references cited therein). The vessel is equipped with a molybdenum furnace. Two S-type thermocouples were used to monitor the temperature and the gradient in the hotspot was controlled to less than 3 °C. Pressure was recorded by a transducer calibrated against a Heise-Bourdon tube gauge (precision of 1.5-2.0 MPa).

The use of Ar-H_2 gas mixtures in the IHPV allows the imposition of variable redox conditions (f_{O2}) depending on the X_{H2} in the mixture. The equilibrium constant (K_w) of the reaction

$H_2O=H_2+½ O_2$, at any given temperature and pressure, allows determination of f_{O2}, if f_{H2} and f_{H2O} in the capsules are known (i.e., X_{H2} in the Ar-H_2 mixture and X_{H2O} in the fluid). A few experiments (R3, R9, and R5) used only Ar gas for pressurization; under such conditions, the redox state was fixed by the intrinsic fH_2 of the pressure vessel which is estimated to be at $\Delta NNO \geq 2$ (Martel et al., 1999).

Tubes of $Au_{80}Pd_{20}$ (Ø 3 mm outer diameter) were loaded with the powdered glass starting material. A series of hydrous saline solutions were prepared with different Cl concentrations, ranging from ~ 0.17 to ~ 20 m Cl, added as NaCl and KCl. In order to minimize possible cation exchange between the fluid and the melt, the molar Na/K ratio of the starting solutions was maintained close to that of the silicate starting material (~ 2.7). A set of experiments was prepared using $Ag_2C_2O_4$ as the source of CO_2 to create a mixed H_2O-CO_2 fluid phase. A single anhydrous capsule was prepared to perform an experiment (R9-2) at 100 MPa and a nominal f_{O2} of NNO≥2 by adding the same chlorine content (as NaCl) as the hydrous experiment R9-1 (Table 2).

For all experiments, the initial fluid/powder mass ratio never exceeded 0.1 in order to minimize the amount of silicates dissolved in the fluid phase. After loading, capsules were sealed by welding without volatile loss, and stored in an oven at 120 °C overnight to check for possible leaks.

All the experiments were performed at temperatures high enough to ensure superliquidus conditions: 1260± 5 °C at 1 MPa and at 1200 °C at higher pressures. Experimental durations varied from 2 to 12 hours (see Table 2). At 1 MPa, experiments of different duration demonstrated that 2 hours are enough to achieve near equilibrium (Fig. 2), as detailed below. At the end of the experiment, the capsules were isobarically quenched by supplying an electrical current to a quench wire resulting in the drop of the sample holder down into the cold part of the vessels. Quench rate was ~ 400 °C/s in the 1 MPa autoclave and 300 °C/s in the IHPV (see Di Carlo et al., 2006).

The capsules were then weighed after each experiment to check for possible leaks and the glass was extracted from the capsule, embedded in epoxy for EMPA analysis and doubly polished for FTIR analysis.

2.4 Major element and Cl analytical techniques

Experimental run products (all glasses) were analyzed by EPMA at McGill University and in Orléans using the BRGM-ISTO joint analytical facilities. At McGill, the run products from the 1 MPa experiments were analyzed with a JEOL 8900 electron microprobe at an accelerating voltage of 15 kV and a 10 nA beam current with a 10-μm defocused beam. Counting time on the peak was 20 s for major elements and 60 s for Cl; backgrounds were measured for one-half (½) of the counting times used on the peaks. A basaltic glass was used as standard for Si, Ti, Al, Fe, Mg, Ca and Na; a rhyolitic glass for K; spessartine for Mn; fluorapatite for P; and vanadinite for Cl (Cl = 2.6 wt.%). The analytical parameters were checked against a standard glass (KE12) containing 0.33 wt.% Cl, which was reproduced to within 10% relative. Sodium loss was checked at these conditions on KE12 and on one of the experiments for counting times between 60 and 120 s and displayed no more than ~ 5 relative % of Na-loss.

At ISTO, the run products of the 25 to 200 MPa experiments were analyzed with either a Cameca Camebax or a Cameca SX 50 electron microprobe. Major elements and chlorine were analyzed separately. Analytical conditions were an accelerating voltage of 15 kV and beam current of 10 nA; the counting time on peak was 10 s for major elements, and 60 s for chlorine. Three standards with known Cl concentrations were analyzed: vanadinite (Cl = 2.6 wt.%), chlorine-apatite (Cl = 6.8 wt.%) and a rhyolitic glass from Eburru volcano (Cl = 0.4 wt.%; Scaillet & Macdonald, 2001). The Cl concentrations in the experimental run-product glasses were determined by applying a linear calibration equation based upon the Cl-counts versus Cl-content of these three standards.

The relative analytical uncertainties using the conditions in the two laboratories are similar to each other: 1% (SiO_2, Al_2O_3, CaO), 3% (FeO, MgO, TiO_2) and 5% (MnO, Na_2O, K_2O, P_2O_5).

In order to verify the homogeneity of the experimental glasses at all pressures, 2 to 3 chips of glass were randomly selected from each capsule, mounted in epoxy (a few capsules of the 1-MPa experiments were entirely embedded) and at least 10 analyses per chip were made. The low standard deviations of these analyses (Tables 2-3) show that the experimental products were homogeneous with respect to their major elements and chlorine concentrations.

2.5 H_2O and CO_2 analysis

Analyses of water in the 1-MPa run-product glasses were performed by Secondary Ion Mass Spectroscopy with a Cameca IMS 4f at the Istituto di Geoscienze e Georisorse (IGG) in Pavia, Italy, using a beam of primary ions $^{16}O^{-}$ at an accelerating voltage of 12.5 keV and a current of 9.5 nA with a spot diameter of 10 – 15 μm. Samples were degassed in the ion-probe sample chamber at P<1 Pa and T ~ 50 °C for 14 hours, before the onset of the analytical session together with the standards. Water was determined by measuring the signal of $^{1}H^{+}$, with $^{30}Si^{+}$ as the internal standard. The analysis of H as ions at medium to high energies reduces the background of H and significantly improves the quality of the analyses (Ottolini et al., 1995 and references cited therein). Basaltic glasses with well-determined water contents (ranging from 0.09 to 0.16 wt.%, Ottolini et al. 1995 and from 1 to 3.20 wt.%, CNR-IGG internal standards) were used as primary standards for H^{+}, and amphiboles were used as secondary standards (Ottolini et al. 1995). The uncertainty on the measurements is estimated to be ~ 10 % relative.

Water dissolved in glasses from experiments at 25 to 200 MPa was analyzed by Fourier transform infrared spectrometry (FTIR) using the bands at 5200 cm^{-1} and 4500 cm^{-1}. The spectra were taken on doubly polished chips of glasses (thickness ~ 100 – 300 μm) using a Nicolet 760 Magna FTIR instrument with an attached optical microscope equipped with a liquid N_2 cooled

MCT/A detector (mercury cadmium telluride detector). Resolution was set to 2 cm^{-1}. A white-light source and a CaF$_2$ beamsplitter were employed in the near-IR region (2000-8000 cm^{-1}). Three to seven spots on each sample were analyzed and spectra were obtained on a 100-micron diameter region by accumulating 512 scans in the range 2000-8000 cm^{-1}; the results were then averaged. The thickness of the samples was measured by using a micrometer whose accuracy is +/- 3 μm. Densities, which depend on the concentration of water dissolved, were corrected using the calibration of Lesne (2008) for Etna hydrous glasses, in agreement with Richet et al. (2000). Molar absorption coefficients from Dixon et al. (1995) were used: $\varepsilon_{H2O} = 0.62$ and $\varepsilon_{OH} = 0.67$ L cm^{-1} mol^{-1} and a tangential baseline correction has been used. The accuracy of our FTIR analysis is estimated to be ≤ 20 relative% for total H$_2$O.

Dissolved carbonate concentrations were also measured by FTIR for samples containing the three volatiles Cl, H$_2$O and CO$_2$ (R13, R17, and R19). In this case, a Globar source and a KBr beamsplitter were employed in the mid-IR region. To minimize the contribution of atmospheric CO$_2$ to the MIR spectra, the sample stage of the IR microscope was shielded and purged with dry air. The concentration was determined from the heights of baseline-corrected peaks of CO$_3^{2-}$ at 1530 and 1430 cm^{-1}. First, we subtracted the spectrum of a CO$_2$-free, hydrous basaltic glass synthesized at 100 MPa and 1200 °C, then we fitted the spectra with tangential baselines. The molar absorption of 375 from Dixon et al. (1995) was used. Unfortunately, this method failed for the experiment performed at 25 MPa (R31), probably due to the very low amount of dissolved CO$_2$. In this case, we calculated the maximum CO$_2$ expected by using the empirical relations between dissolved H$_2$O and CO$_2$ and their fugacities, as developed by Lesne (2008) for Mt. Etna basaltic melts. This approach does not take into account the possible effect of Cl on the solubility of the other volatiles, and it yields the maximum CO$_2$ concentration that can be expected in our melt. The low concentrations of CO$_2$ calculated for the experiment R31 at 25 MPa (between 24 and 82 ppm), together with the interference of the H$_2$O peak at 1630 cm^{-1} with the peaks of carbonates at high X_{H2O}, both suggest that the real content must be near the detection limit of the instrument (which for

hydrous basalts is between 50 and 100 ppm). In any case, the low CO_2 concentrations in the glasses only marginally affect the mass balance calculations used to retrieve the halogen content in the fluid phase.

2.6 Estimation of oxygen fugacity during the experiments

The experiment performed at 1 MPa by adding 5000 ppm S to the basalt, allowed us to evaluate the f_{O2} of the 1 MPa dataset by using the thermodynamic model of Moretti & Ottonello (2005) which accounts for the compositional dependence of sulfur speciation when solving the equilibrium constant of the following reaction

$$S^{2-} + 2O_2 = SO_4^{2-} .$$
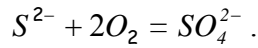
To this end, we determined the shift in the sulfur $K\alpha$ x-ray emission peak (i.e., $\Delta\lambda Sk\alpha$), and found a ratio of S^{6+}/S_{TOTAL} equal to 0.79. At the experimental T of 1260 +/- 5 °C this corresponds to an oxygen fugacity 0.3 log units below the nickel-nickel oxide buffer, or $\Delta NNO = -0.3$ (see Moretti & Baker, 2008).

In order to evaluate the redox conditions of the higher pressure experiments (Table 4), we assume that the following equilibrium is established inside each capsule:

$$H_2 + \frac{1}{2}O_2 = H_2O \qquad (1)$$

and

$$\frac{1}{2}\log f_{O2} = \log \frac{f_{H2}}{f_{H2O}} + \log K_w \qquad (2)$$

The thermodynamic data of Barin et al. (1977) were used to compute the equilibrium constant K_w. The f_{H2}/f_{H2O} ratio imposed to each run was used to recalculate f_{O2} using equation 2. To perform the calculations the values of the fugacity coefficients γ_{H2} and γ_{H2O} were determined with the

SUPERFLUID code (Belonoshko et al., 1992). In order to calculate the oxygen fugacity in CO_2-bearing experiments it was assumed that chlorine does not appreciably affect H_2O and CO_2 mixing properties. The fugacity coefficient of H_2 in the mixture (γ_{H2}) was then recomputed, based on the proportion P_{H2}/P_{TOT} in each experiment. These calculations demonstrate that for the experiment containing CO_2 at 100 MPa, the oxygen fugacity of the fluid with $X_{CO2} = 0.3$ is 0.3 log units lower than the CO_2-free fluid (compare R17 and R14 on Table 4; see also Webster et al., 1987).

When no H_2 was introduced into the IHPV, the oxygen fugacity of the hydrous experiments in the IHPV was ΔNNO $\geq$ +2 (Martel et al., 1999). Assuming that CO_2 affects oxygen fugacity in the same way as above, the unbuffered f_{O2} for the experiment at 100 MPa and H_2O+CO_2 (R13) would be at NNO $\geq$ 1.7 rather than NNO $\geq$ + 2.

The oxygen fugacity of the experiments reported in this paper varies between $\geq$ NNO+2 to NNO-0.3, but for simplicity two groups will be considered in the discussion below, the NNO+2 group (from $\geq$ NNO+2 to 1.7<NNO<2) and the NNO group (from NNO-0.3 to NNO+0.8).

2.7 Mass-balance calculations

Due to the complexity of extracting and analyzing extremely small quantities of quenched fluid from each experiment, the chlorine concentrations in the fluid phase at run conditions were calculated by mass balance following the approach used by Signorelli and Carroll (2000):

Mass of chlorine in the fluid = Mass of chlorine initial – Mass of chlorine in final glass

where

Mass of chlorine initial = $C_{Cl}^{fl,i}$ x $M^{fl,i}$ + $C_{Cl}^{m,i}$ x $M^{m,i}$

and

Mass of chlorine in final glass = C_{Cl}^{m} x ($M^{m,i}$ + M_{alk}^{m} + M_{H2O}^{m} + $M_{Cl}^{m,i}$ – M_{DS}^{fl} + M_{CO2}^{m}),

where $C_{Cl}^{fl,i}$ is the initial concentration of chlorine in $M^{fl,i}$ mass of fluid added; $C_{Cl}^{m,i}$ is the initial concentration of the chlorine in the silicate powder; C_{Cl}^{m} is the final concentration of chlorine in the glass melt; $M^{m,i}$ is the initial mass of silicate glass powder; M_{alk}^{m} is the final mass of alkali in the glass; M_{H2O}^{m} is the mass of water in the final glass; $M_{Cl}^{m,i}$ is the mass of chlorine in the initial rock powder; M_{DS}^{fl} is the mass of silicate dissolved in fluid; and M_{CO2}^{m} is the final mass of CO_2 dissolved in the final glass. The concentration of chlorine in the fluid phase was then calculated taking into account the masses of all the volatiles, i.e. Cl, H_2O, and CO_2 when present.

The mass of alkalis in the melt gained or lost during the experiments (M_{alk}^{m}) was calculated from Na_2O and K_2O concentrations in the glass, considering that the masses of other elements dissolved in the fluid (M_{DS}^{fl}) remain negligible (due to the experimental procedure that constrained the fluid/glass ratio to less than 0.1). The mass of water dissolved in the melt was determined by direct H_2O analysis (FTIR or SIMS) in the experimental glasses. The mass of CO_2 in the final glass was determined by FTIR, for all the experiments (other than R31 at 25 MPa, as discussed above). Once the mass of chlorine is known in the melt and fluid phases, these values are divided by the total mass of each phase to calculate the chlorine concentrations and the partition coefficients.

The total uncertainty ($\pm 1\sigma$) associated with the calculated mass of chlorine in the fluid phase is the result of weighing errors associated to the balance and uncertainties in the analytical estimations of water, chlorine and alkalis in the final glass (Table 2). The average uncertainty of the calculated partition coefficients is estimated at no more than 30 percent.

3. Results

The experimental run conditions, the measured chlorine concentrations in the experimental glasses, the calculated concentrations in the bulk fluid phase and the major-element compositions of run-product glasses are listed in Tables 2 and 3.

All experimental run products were glasses; those at 1 MPa were more vesicular (no more than 10 volume%) than those from higher pressure (Fig. 1). Only a few runs (R3 and R14-1) contained

about 10 volume% of small bubbles, probably formed during quench. The presence of bubbles might affect the H_2O concentrations in those glasses even though we carefully tried to avoid them during analysis. However the low standard deviations of the measured water concentrations indicate that any heterogeneity was within the analytical uncertainty. Runs R5 and R13-8 contained crystals which, due to their small size, were not analyzable. Based on the backscattered electron images and, taking into account that those experiments were performed at oxidizing conditions, we infer that they are most probably iron oxides. The maximum modal proportion of crystals was in all cases less than 10%.

To check the attainment of equilibrium in the experiments, we compared the results of the –in and –out (i.e., reversal) experiments and we also performed experiments of different durations at 1 MPa. Comparison of the experiments Cl-McG3 and Cl-McG4 (Table 2a) shows convergence of partition coefficients within uncertainty. Experimental durations from 1 to 12 h demonstrate that chlorine concentrations in the melts are within uncertainty of each other (Fig. 2), and thus support the use of 3 to 4 h durations for experiments at higher pressures.

Chlorine concentrations in our basaltic glasses range from 0.13 to 1.94 wt.%. The FeO concentration of the experimental products ranges between 10 and 7.7 wt.%, and most experimental crystal-free-glasses contain $\geq$ 90% of the FeO content of the starting material, demonstrating that the experimental procedure was successful in minimizing Fe-loss toward the capsules.

H_2O concentrations in the quenched glasses vary from 0.13 wt.% in the 1 MPa experiments up to 6.11 wt.% in the 200 MPa experiments. CO_2 contents raise up to 414 ppm depending on pressure (Table 2b). The calculated apparent Cl concentrations of the fluid phase in the experiments range from 0 to 74.75 wt.%.

Fluid-melt partition coefficients of Cl ($D^{f/m}$) were calculated with the measured compositions of Cl in the glasses and the calculated concentrations of Cl in the fluid phase on a weight percent basis. For each group of runs at equivalent temperature, pressure, and fluid composition (i.e., $Cl+H_2O$ or $Cl+H_2O+CO_2$), the Cl concentrations in the melt and fluid phases were plotted against

each other (Fig. 3). Each set of measurements produces a trend that is broadly linear only at low Cl concentrations, typically up ~ 0.4 wt.% Cl (with the exception of the 1 MPa experiments). At higher concentrations, Cl in the fluid follows a parabolic increase with Cl in the melt or it produces a break-in-slope, indicative of the possible occurrence of an additional phase in the system or complex activity-composition relationship (cf. Carroll & Webster, 1994, and references therein). There is indeed both theoretical and experimental evidence that either a low-density hydrous vapor, an hydrosaline liquid (i.e., a brine), or both, can coexist with silicate melts in a H_2O-Cl–bearing system up to 1000 °C at least, depending on P, T and X_{Cl} (e.g., total Cl content) conditions (Shinohara et al., 1989; Lowenstern, 1994; Webster, 2004; Webster & Mandeville, 2007; Driesner & Heinrich, 2007).

Three tests were performed so as to discriminate between the presence of a single aqueous fluid phase or of two fluid phases (brine + aqueous fluid) in our experiments. The first test was an optical inspection of each glass after the experiments. In no case was any saline fluid inclusion indicative of a quenched brine observed. The second test was to use alkali mass balance, assuming only a silicate melt and an aqueous fluid; in practice we compared the alkali concentrations measured in the experimental glasses with the initial bulk concentration of alkalies in the system (given by the starting glass and the solutions added); the results are shown in Fig. 4. The charges falling in the positive region are unambiguously enriched in Na and K, and the experimental conditions were possibly conducive to brine formation. On the other hand, when the alkali mass balance yields negative results, it suggests that all the Na and K added before the experiments as chloride were largely incorporated in the melt which was therefore in equilibrium with a C-O-H-Cl-rich vapor fluid phase. This second case is likely to be especially true for those samples with the lowest concentrations of Cl in the solutions. The third test was to compare the measured concentrations of water and Cl in the glass. For each experimental condition of temperature and pressure, we found that the water concentration in the melt was approximately constant and independent of the Cl concentration (Fig. 5). Although in the presence of a brine such a behavior is

also expected, most of our experiments were at initial Cl concentrations far below saturation with a brine which suggests that only melt+vapor coexisted (cf. Webster et al., 1999).

Based upon these three tests we conclude that the majority of experiments only contained two phases: a silicate melt and an aqueous fluid. However, we note that some experiments reach apparent Cl contents in the fluid of greater than 50 wt.%; for those experiments brine precipitation cannot be excluded.

The averaged partition coefficients at each pressure (Table 5) were derived by linearly fitting the low concentration data only (i.e., data up to the change in slope, ≤ 0.4 wt.%). For experiments with only H_2O+Cl, at $f_{O2} \geq$ NNO+2, $D_{Cl}^{f/m}$ ranges between 4 at 50 MPa to 13 at 100 MPa, while at ~NNO, the partition coefficient ranges between 11-14, at 1 and 25 MPa, respectively, and 6 at 200 MPa. For H_2O+Cl+CO_2 experiments, the partition coefficient ranges between 3 to 8 at ~NNO.

4. Discussion

4.1 Inferences on chlorine solubility in basaltic melts

As discussed above, the Cl concentrations of our glasses are not representative of Cl solubility (defined here as the saturation of the melt with a brine) strictu sensu, since the experiments were mainly performed at Cl-undersaturated conditions in an attempt to calculate Nernst-type partition coefficients between two phases. Although the behavior of chlorine is far more complex, this simplification has been shown to be useful for the modeling of chlorine behavior at Etna (Spilliaert et al., 2006a, b) and basaltic systems in general (Webster et al., 1999), given the low concentration of Cl in primitive basaltic melts. Because of this, a direct comparison of our results with previous experimental investigations of Cl solubility in natural silicate melts of different composition is not straightforward. Our measurements allow us, however, to make qualitative considerations on Cl solubility at the investigated conditions.

It is widely recognized that chlorine solubility is strongly dependent on silicate melt composition (Webster & De Vivo, 2002; Signorelli & Carroll, 2000; Webster et al., 1999; Métrich

& Rutherford, 1992; Malinin et al., 1989), and Webster (1997) demonstrated that Cl solubility increases with decreasing H_2O abundance in felsic to intermediate melts. The only nominally anhydrous, Cl-saturated experiment we attempted was at 100 MPa (R9-2; Table 3) but this quenched glass ended up containing 1.64 wt.% dissolved H_2O. Nevertheless, it demonstrates that H_2O-poor silicate melts dissolve higher Cl concentrations than H_2O-saturated ones. Indeed, even though the added concentration of Cl ($\sim$ 2 wt.%) was the same in the nominally anhydrous R9-2 and in the hydrous R9-1, the nominally anhydrous glass contains $\sim$ 60 % more Cl than the H_2O-saturated one (Table 2).

Webster & De Vivo (2002) developed a solubility model to compute the maximum concentration of Cl in different melts at 200 MPa. With this model, and using the melt compositions of the only experiment we performed at this pressure (R34), we calculate Cl solubilities between 2.7 and 2.8 wt.%, which are significantly higher than the maximum Cl concentration we measured in this study (1.46 wt.%). Such a large difference strongly suggests that at 200 MPa the system did not reach brine saturation.

Figure 3A shows a clear break-in-slope for the 1-MPa experiments at $\sim$ 1.3 wt.% Cl in the melt. This break in slope is suggestive of saturation of the silicate melt with a chloride brine at Cl concentrations in the melt above 1.3 wt.%. Such a break-in-slope is not observed for the other sets of experiments at different pressures and similar redox conditions (Fig. 3A and Fig. 3B). The maximum Cl concentrations measured in the experiments involving H_2O and Cl are: 0.40 wt.% at 25 MPa, 0.78 wt.% at 50 MPa, 1.94 wt.% at 100 MPa, and 1.46 wt.% at 200 MPa. The maximum concentration reached at 100 MPa is $\sim$ 1 wt.% lower than the theoretical solubility calculated at 200 MPa with the Webster & De Vivo (2002) model. All these observations are further evidence that the experiments used to calculate the partition coefficients (i.e., most of our experiments) were not saturated in brine; the sole exceptions are one experiment at 1 MPa (discussed above) and one at 100 MPa, containing 1.94 wt.% of Cl in the melt and 74.75 wt.% Cl in the fluid phase.

Comparison between the results obtained at different oxygen fugacities and at pressures of 50 MPa and 100 MPa (Fig. 6), shows that f_{O2} does not exert any significant influence on Cl partitioning at low Cl concentrations in the melt. At Cl contents higher than 0.3 wt.%, a systematic, yet small, tendency of increasing Cl partitioning toward the fluid phase at low f_{O2} is apparent.

The effect of CO_2 on Cl partitioning appears more striking (Fig. 7): increased Cl affinities for the melt (e.g., lower vapor-melt partition coefficients) are observed in CO_2-bearing runs, compared to CO_2-free runs performed at similar P-T-X conditions. Webster & Holloway (1988) and Botcharnikov et al. (2007) already reported such behavior for rhyolitic and andesitic melts, respectively. In particular, Webster & Holloway (1988) interpreted the effect as due to a decrease of the mean dielectric constant of the fluid phase and to an increase of Cl activity in the fluid. In fact, it is recognized in the study of ore and igneous fluids (Holloway, 1987; Brimhall & Crerar, 1987) that the solubility of chemical species in hydrothermal fluids is a function of several properties of the fluid such as the dielectric constant, which in turns depends on the dipole moments of the fluid components. Variations in the composition of the fluids affect the dipole moment of the species in the fluid and consequently the solvating capacity of the fluid.

4.2 Pressure-dependence of fluid/melt chlorine partitioning

Previous studies on chlorine solubility in H_2O-bearing felsic melts of different compositions (mainly phonolitic and rhyolitic) have demonstrated a negative correlation between Cl solubility and pressure, which in turn reflects an increase of $D_{Cl}^{f/m}$ with P (Shinohara et al., 1989; Métrich & Rutherford, 1992; Signorelli & Carroll, 2000; Signorelli & Carroll, 2002). Such a pressure dependence has been interpreted as due to the large negative partial molar volume of NaCl in the vapor phase (for details see Shinohara et al., 1989 and Signorelli & Carroll, 2002), and to the strong non-ideality of the H_2O-NaCl system. In contrast, the effect of pressure on Cl solubility in mafic melts is far from being constrained: a positive dependence of Cl solubility on pressure was reported

for anhydrous basalts (Webster et al., 1999; Malinin et al., 1989), whilst H_2O-rich basaltic melts have been experimentally investigated only at high pressure (200 MPa; Webster et al., 1999; Stelling et al., 2008; Chevychelov et al., 2008), and no Cl solubility vs. P relation has ever been established.

As explained above, we derived fluid/melt partition coefficients of Cl from experiments with a maximum concentration of 0.4 wt.% of Cl in the melt. In this way, we obtained the $D_{Cl}^{f/m}$ values displayed in Table 5 at the different experimental conditions. Fig. 8 shows a slight negative dependence of $D_{Cl}^{f/m}$ with P for the experiments at $f_{O2} \sim$ NNO with the binary H_2O-Cl fluid. This result contrasts with those of previous studies demonstrating an increase of $D_{Cl}^{f/m}$ with pressure (Signorelli & Carroll, 2000, 2002). This is only an apparent disagreement because we derived our partition coefficients using data at low Cl concentration, in order to avoid the effect of brines or excess of NaCl in the fluid. In addition, as pointed out by Shinohara (2009, this issue), the ratio HCl/NaCl in the fluid phase is negatively dependent on pressure, and dramatically increases at pressures lower than 100 MPa, where most of our experiments were performed. If HCl was the main Cl gaseous species in the fluid phase at the experimental conditions, particularly in the low P range, this might have masked the effect on $D_{Cl}^{f/m}$ played by the negative partial molar volume of NaCl in the vapor phase. On the contrary, experiments performed at higher oxygen fugacity seem to behave differently (see also previous section), and lack any significant pressure dependence, at least in the range investigated. The introduction of CO_2 in the system also tends to diminish any pressure dependence (Table 5 and Fig. 8). This effect can be related to the enlargement of the P-T-X range of the immiscibility gap in H_2O-salt-bearing fluid systems when CO_2 is added (Shmulovich & Graham, 2004).

Stelling et al. (2008) recently reported Cl partitioning and solubility experiments in hydrous basaltic melts from Mount Etna at 200 MPa, oxygen fugacity an order of magnitude above that of the fayalite-quartz-magnetite buffer, and temperatures between 1050 and 1250 °C. The authors reported $D_{Cl}^{f/m}$ at the investigated conditions ranging between 0 and 24. Comparison between the

two sets of data (Fig. 9) shows that, at similar Cl concentrations in the melt, the fluid phase in our experiments is richer in Cl than in Stelling et al (2008), (i.e., for 0.5 wt.% Cl in the melt, Stelling et al. find 0.59 wt.% Cl in the fluid phase, while we find 5.5 wt.%). Sensitivity tests of the mass-balance calculations revealed that the Cl concentrations in the fluid are significantly affected by even small variations in one of the measured parameters. For example, changing the Cl concentration of the starting material by 0.03 wt.% for R34-3, decreases the Cl content in the fluid to 1.16 wt.%. Thus, this sensitivity can easily explain difference in $D_{Cl}^{f/m}$ between this study and that of Stelling et al., (2008). This observation illustrates, however, the difficulties in accurately constraining Cl behavior in magmas. This mass-balance sensitivity is one of the reasons we derive our results from multiple experiments with varying Cl concentrations in the melt and fluid.

Comparing our results to other studies of Cl partitioning between hydrous fluids and basaltic melts at 200 MPa (Webster et al., 1999; Mathez & Webster, 2005; Stelling et al., 2008) demonstrates good agreement (Fig. 10). However, two experiments by Stelling et al (2008) and one by Webster et al. (1999) display partition coefficients approximately one-third of those found in this study. The source of this disagreement remains enigmatic as the concentrations of Cl in the melts with low partition coefficients (see Fig. 10) are similar to those of melts with the higher ones.

Fig. 10 demonstrates the agreement among the partitioning data available for basalts at high pressure and that, for Cl concentrations in the melt between 0.51 and 1.83 wt.%, at 200 MPa, $D_{Cl}^{f/m}$ is found to range between 1.5 and 7.0.

5. Implications for volcanic degassing of Etna

Although the development of a rigorous model of volatile degassing is not the aim of this study, our experimental results can be used for a first-order calculation of Cl contents in magmatic

gases in equilibrium with Etna magmas over a range of pressures. These calculated compositions can then be compared with natural data on Cl concentrations in volcanic gases from Etna.

Fig. 8 shows, for the experiments with H_2O and Cl at $f_{O2} \sim$ NNO, the pressure dependence of the weight-percent partition coefficient can be expressed by the equation:

$$D_{Cl}^{f/m} = 12.732*P^{-0.0853} \qquad (3)$$

where P is in MPa.

Using equation 3 we calculate the partition coefficients in the pressure range 200 - 0.1 MPa. Then, assuming closed-system degassing and an initial Cl concentration of 0.23 wt.% Cl (Métrich et al., 1993) and 3.5 wt.% H_2O (Spilliaert et al., 2006b) dissolved in the melt, we calculated the fluid composition for Cl over the same pressure range (Fig. 11). Calculations show that Cl makes up a very small fraction of the magmatic gas phase exsolved by Etna's magmas upon their ascent (Fig. 11), in agreement with measured volcanic gas data. It appears that the typical Cl concentration in Etna's volcanic gases (~2 wt.%, see compilation in Table 2 from Aiuppa et al., 2009, this issue) corresponds to our model-predicted Cl concentration at pressures shallower than 30 MPa. This is in broad agreement with results of recent studies (Aiuppa et al., 2004, 2007) showing that the chemistry of quiescent gas discharges from Etna are representative of "frozen equilibrium compositions" attained at shallow depths in volcanic conduits. It thus appears that studying Cl degassing sheds light on only the shallowest part of volcanic degassing path of basaltic volcanoes, as suggested by Aiuppa (2009, this issue).

The above simulation does not include CO_2 which is an important volatile species at Etna. Incorporation of CO_2 would require, however, the knowledge of fugacity-composition relationships of all species, which are not all currently available. This is the next goal to be achieved in order to rigorously model magmatic degassing at basaltic volcanoes.

6. Conclusions

Significant advances in the comprehension of volatile behavior in magmatic and volcanic systems have been achieved in the past decades. The acquisition, analysis and interpretation of large datasets from natural systems (i.e., volcanic gases, melt and fluid inclusions), combined with experimental determinations of volatile behaviors in magmas, have resulted in the development of models aimed at understanding volcanic degassing. These models (e.g., Moretti et al., 2003) have most often been restricted to the C-H-O-S system, because relevant data (e.g., solubility, vapor-melt partitioning) required to model halogen behavior have been in large part lacking.

Our measurements provide the basis for a better understanding of the modes, timing and rates of Cl degassing in basaltic systems, which have been a matter of increasing interest in recent years (Spilliaert et al., 2006b; Aiuppa et al., 2009, this issue). Our data confirm earlier findings (Webster et al., 1999) that Cl can be dissolved at wt.% levels in basaltic magmas at shallow crustal conditions. They also demonstrate that Cl has a high affinity for the H_2O-bearing vapor phase exsolved by decompressing basaltic magmas upon ascent in the upper crust. Altogether, our experiments indicate that Cl concentrations will be ~10 times higher in the vapor phase than in the coexisting basaltic melt. We also demonstrate that Cl partitioning between fluid and melt is highly dependent on the composition of the fluid phase and, to a lesser extent, on pressure and oxygen fugactity. At f_{O2} near NNO and in the H_2O-Cl system, Cl fluid-melt partition coefficients ($D_{Cl}^{f/m}$) decrease with increasing pressure, and are slightly higher than in more oxidizing conditions. Adding CO_2 to the system, at NNO, has the general effect of reducing the partition coefficients, and minimizing any affect of pressure. We stress, however, that most experiments were performed at supercritical conditions, and are thus representative of Cl partitioning between melt and a hydrous vapor phase only; solubility measurements at much larger Cl contents (e.g., Stelling et al., 2008) are still required to fully explore the basalt-Cl-H_2O-CO_2 system, in particular where the formation of Cl-bearing brines is likely to occur.

Acknowledgements

References

Aiuppa, A., 2009-this issue. Degassing of halogens from basaltic volcanism: Insights from volcanic gas observations. Chem. Geol. doi:10.1016/j.chemgeo.2008.08.022.

Aiuppa, A., Federico, C., Paonita, A., Pecoraino, G., Valenza, M., 2002. S, Cl and F degassing as an indicator of volcanic dynamics: the 2001 eruption of Mount Etna. Geophys. Res. Lett. 29-11, doi:10.1029/2002GL015032.

Aiuppa, A., Federico, C., Giudice, G., Guerrieri, S., Paonita, A., Valenza, M., 2004. Plume chemistry provides insights into mechanisms of sulfur and halogen degassing in basaltic volcanoes. Earth. Planet. Sci. Lett. 222, 469-483.

Aiuppa, A., Moretti, R., Federico, C., Giudice, G., Gurrieri, S., Liuzzo, M., Papale, P., Shinohara, H., Valenza, M., 2007. Forecasting Etna eruptions by real-time observation of volcanic gas composition. Geology 35, 1115-1118.

Aiuppa, A., Baker D.R., Webster J.D., 2009-this issue. Halogens in volcanic systems. Chem. Geol. doi:10.1016/j.chemgeo.2008.10.005

Allard, P., Burton, M., Mure, F., 2005. Spectroscopic evidence for a lava fountain driven by previously accumulated magmatic gas. Nature 433, 407–410.

Alletti, M., Baker, D.R., Freda, C., 2006. Fluid/melt partitioning coefficients of chlorine in basaltic melt. Geophys. Res. Abstracts, Vol. 8, 08823.

Barin, I., Knacke, O., Kubaschewsky, O., 1977. Thermochemical properties of inorganic substances. Supplement. "Springer – Verlag".

Belonoshko, A.B., Shi P., Saxena S.K., 1992. SUPERFLUID: A FORTRAN77 program for calculation of Gibbs free energy and volume of C-H-O-N-S-Ar mixtures. Comput. Geosci. 18, 1267-1269.

Bonaccorso, A., Calvari, S., Coltelli, M., Del Negro, C., Falsaperla, S., 2004. Mt. Etna: Volcano laboratory: AGU Geophys. Monograph 143, 369.

Botcharnikov, R.E., Behrens, H., Holtz, F., Koepke, J., Sato H., 2004. Sulfur and chlorine solubility in Mt. Unzen rhyodacitic melt at 850 °C and 200 MPa. Chem. Geol. 213, 207-225.

Botcharnikov, R.E., Holtz, F., Behrens, H., 2007. The effect of CO_2 on the solubility of H_2O-Cl fluids in andesitic melt. Eur. J. Mineral. 19, 671-680.

Boudreau, A.E., Mathez, E.A., McCallum, I.S., 1986. Halogen geochemistry of the Stillwater and Bushveld Complexes: Evidence for transport of the platinum-group elements by Cl-rich fluids. J. Petrol. 27, 967-986.

Brimhall, G.H., Crerar, D.A., 1987. Ore fluids; magmatic to supergene. Rev. Mineral. Geochem. 17, 235-321.

Burgisser, A., Scaillet B., 2007. Redox evolution of a degassing magma rising to the surface. Nature, 445, doi:10.1038/nature05509.

Burnham, C.W., 1979. Hydrothermal fluids at the magmatic stage. In: Barnes H.L. (Ed.), Geochemistry of Hydrothermal Ore Deposits. John Wiley & Sons, New York, 34-76.

Carroll, M.R., Webster J.D., 1994. Solubilities of sulfur, noble gases, nitrogen, chlorine and fluorine in magmas. In: Volatiles in Magmas (eds. M. R. Carroll and J. R. Holloway). Rev. Mineral. 30, 231-279.

Chevychelov, V.Y., Botcharnikov, R.E., Holtz, F., 2008. Experimental study of fluorine and chlorine partitioning between fluid and subalkaline basaltic melt. Doklady Earth Sciences, 422, 1089-1092.

De Gori, P., Chiarabba, C., and Patanè, D., 2005, Qp structure of Mount Etna: Constraints for the physics of the plumbing system: J. Geophys. Res. 110, B05303, doi:10.1029/2003JB002875.

Di Carlo, I., Pichavant, M., Rotolo, S.G., Scaillet, B., 2006. Experimental crystallization of a high-K arc basalt: the Golden Pumice, Stromboli Volcano (Italy). J. Petrol. 47, 1317 – 1343.

Dingwell, D.B., Mysen, B.O., 1985. Effects of water and fluorine on the viscosity of albite melt at high pressure: a preliminary investigation. Earth Planet. Sci. Lett. 74, 266-274.

Dixon, J.E., Stolper, E.M., Holloway, J.R., 1995. An experimental study of water and carbon dioxide solubilities in mid-ocean ridge basaltic liquids, Part I. Calibration and solubility models. J. Petrol. 36,1607-1631.

Dolejs, D., Baker, D.R., 2004. Thermodynamic analysis of the system $Na_2O-K_2O-CaOAl_2O_3- SiO_2-H_2O-F_2O_{-1}$: stability of fluorine-bearing minerals in felsic igneous suites. Contrib. Mineral. Petrol. 146, 762-778.

Driesner, T., Heinrich, C.A., 2007. The system H_2O-NaCl. Part I: Correlation formulae for phase relations in temperature-pressure composition space from 0 to 1000°C, 0 to 5000 bars, and 0 to 1 X_{NaCl}. Geochim. Cosmochim. Acta 71, 4880-4901.

Francis, P., Burton, M., Oppenheimer, C., 1998. Remote measurements of volcanic gas compositions by solar occultation spectroscopy. Nature, 396, 567–569.

Giordano, D., Romano C., Dingwell D.B., Poe B., Behrens H., 2004. The combined effects of water and fluorine on the viscosity of silicic magmas. Geochim. Cosmochim. Acta, 68, 5159-5168.

Heinrich, C.A., 2005. The physical and chemical evolution of low-salinity magmatic fluids at the porphyry to epithermal transition: a thermodynamic study. Miner. Deposita 39, 864-889.

Holloway, J.R., 1987. Igneous fluids. In: Carmichael, I. S. E. & Eugster, H. P. (eds) Thermodynamic Modelling of Geological Materials: Minerals, Fluids and Melts. Mineral. Soc. Amer., Rev. Mineral. 17, 211–233.

Iwasaki, B., Katsura, T., 1967. The solubility of hydrogen chloride in volcanic rock melts at a total pressure of one atmosphere and at temperatures of 1200°C and 1290°C under anhydrous conditions. Bull. Chem. Soc. Japan. 40, 554-561.

Lange, R.A., 1994. The effect of H_2O, CO_2 and F on the density and viscosity of silicate melts. In Volatiles in Magmas (eds. M. R. Carroll and J. R. Holloway). Rev. Mineral. 30, 331-369.

Lesne P., 2008. Etude expérimentale de la solubilité des volatils C-H-O-S dans les basaltes alcalins italiens. Simulations numériques du dégazage chimique : application à l'Etna. PhD thesis, Université d'Orléans.

Lowenstern, J.B., 1994. Chlorine, fluid immiscibility, and degassing in peralkaline magmas from Pantelleria, Italy. Am. Mineral. 79, 353– 369.

Malinin S. D., Kravchuk I. F., Delbove F., 1989. Chloride distribution between phases in hydrated and dry chloride-aluminosilicate melt systems as a function of phase composition. Geochem. Int. 26, 32–38.

Manning, D.A.C., 1981. The effect of fluorine on liquidus phase relationships in the system Qz-Ab-Or with excess water at 1kb. Contrib. Mineral. Petrol. 76, 206-215.

Martel, C., Pichavant, M., Holtz, F., Scaillet, B., Bourdier, J.-L., Traineau, H., 1999. Effects of fo_2 and H_2O on andesite phase relations between 2 and 4 kbar. J. Geophys. Res. 104, 29453–29470.

Mathez, E. A., Webster, J. D., (2005) Partitioning behavior of chlorine and fluorine in the system apatite–silicate melt–fluid. Geochim. Cosmochim. Acta 69, 1275–1286.

Métrich, N., Rutherford, M.J., 1992. Experimental study of chlorine behavior in hydrous silicic melts. Geochim. Cosmochim. Acta 56, 607-616.

Métrich, N., Clocchiatti, R., 1996. Sulfur abundance and its speciation in oxidized alkaline melts: Geochim. Cosmochim. Acta 60, 4151–4160.

Métrich, N., Clocchiatti, R., Mosbah, M., Chaussidon, M., 1993. The 1989-90 activity of Etna. Magma mingling and ascent of a H_2O-Cl-S rich basalt. Evidence from the melt inclusions. J. Volcanol. Geotherm. Res. 59, 131-144.

Métrich, N., Allard, P., Spilliaert, N., Andronico, D., Burton, M., 2004. 2001 flank eruption of the alkali- and volatile-rich primitive basalt responsible for Mount Etna's evolution in the last three decades. Earth. Planet. Sci. Lett. 228, 1-17.

Moretti, R., Ottonello, G., 2005. Solubility and speciation of sulfur in silicate melts: The conjugated Toop-Samis-Flood- Grjotheim (CTSFG) model. Geochim. Cosmochim. Acta, 69, 801-823.

Moretti, R., Baker, D.R., 2008. Modeling the interplay of fO_2 of fS_2 along the FeS-silicate melt equilibrium. Chem. Geol. 256, 286-298.

Moretti, R., Papale, P., Ottonello, G., 2003. A model for the saturation of C-O-H-S fluids in silicate melts. Geological Society, London, Special Publication, 213, 81–102.

Ottolini, L., Bottazzi, P., Zanetti, A., Vannucci, R., 1995. Determination of hydrogen in silicates by Secondary Ion Mass Spectrometry. Analyst 120, 1309-1313.

Pennisi, M., Le-Cloarec, M.F., 1998. Variations of Cl, F, and S in Mount Etna's plume, Italy, between 1992 and 1995. Geophys. Res. Lett. 103, 5061–5066.

Richet, P., Whittington, A., Holtz, F., Behrens, H., Ohlhorst, S., Wilke, M., 2000. Water and the density of silicate glasses. Contrib. Mineral. Petrol. 138, 337-347.

Scaillet, B., Macdonald, R., 2001. Phase relations of peralkaline silicic magmas and petrogenetic implications. J. Petrol. 42, 825–845.

Shinohara, H., 2009-this issue. A missing link between volcanic degassing and chloride partitioning experiments. Chem. Geol. (in press).

Shinohara, H., Ilyama, J.T., Matsuo, S., 1989. Partition of chlorine compounds between silicate melt and hydrothermal solutions: I. Partition of NaCl-KCl. Geochim. Cosmochim. Acta 53, 2617-2630.

Shmulovich, K.I. & Graham, C.M., 2004. An experimental study of phase equilibria in the systems H_2O-CO_2-$CaCl_2$ and H_2O-CO_2-NaCl at high pressures and temperatures (500-800 ∘C, 0.5-0.9 GPa): geological and geophysical applications. Contrib. Mineral. Petrol. 146, 450-462.

Signorelli, S., Carroll, M.R., 2000. Solubility and fluid-melt partitioning of Cl in hydrous phonolitic melts. Geochim. Cosmochim. Acta 64, 2851-2862.

Signorelli, S., Carroll, M.R., 2002. Experimental study of Cl solubility in hydrous alkaline melts: constraints on the theoretical maximum amount of Cl in trachytic and phonolitic melts. Contrib. Mineral. Petrol. 143, 209-218.

Spilliaert, N., Allard, P., Métrich, N., Sobolev, A.V., 2006a. Melt inclusion record of the conditions of ascent, degassing and extrusion of volatile-rich alkali basalt during the powerful 2002 flank eruption of Mount Etna (Italy). J. Geophys. Res. 111, B04203, doi:10.1029/2005JB003934.

Spilliaert, N., Métrich, N., Allard, P., 2006b. S-Cl-F degassing pattern of water rich alkali basalt: modelling and relationship with eruption styles of Mount Etna volcano. Earth Planet. Sci. Lett. 248, 772-786.

Stelling, J., Botcharnikov, R.E., Beermann, O., Nowak, M., 2008. Solubility of H_2O- and chlorine-bearing fluids in basaltic melt of Mount Etna at T=1050-1250°C and P=200 MPa. Chem. Geol. doi:10.1016/j.chemgeo.2008.04.009.

Symonds, R.B., Rose, W.I., Bluth, G.J.S., Gerlach, T.M., 1994. Volcanic-gas studies: methods, results and applications. In Volatiles in Magmas (eds. M. R. Carroll and J. R. Holloway). Rev. Mineral. 30, 1-60.

Webster, J.D., 1997. Chloride solubility in felsic melts and the role of chloride in magmatic degassing. J. Petrol. 38, 1793-1807.

Webster, J.D., 2004. The exsolution of magmatic hydrosaline chloride liquids. Chem. Geol. 210, 33– 48.

Webster, J.D., Holloway, J.R., 1988. Experimental constraints on the partitioning of Cl between topaz rhyolite melt and H_2O and H_2O+CO_2 fluids: New implications for granitic differentiation and ore deposition. Geochim. Cosmochim. Acta 52, 2091-2105.

Webster, J.D., Mandeville, C.W., 2007. Fluid immiscibility in volcanic systems. In: Liebscher, A., Heinrich, C.A. (Eds.), Fluid-Fluid Interactions. Rev. Mineral. Geochem., 65, 313–362.

Webster, J.D., Holloway, J.R., Hervig, R.L., 1987. Phase equilibria of a Be, U and F-enriched vitrophyre from Spor Mountain, Utah. Geochim. Cosmochim. Acta, 51, 389-402.

Webster, J.D., Kinzler, R.J., Mathez, A., 1999. Chloride and water solubility in basalt and andesite melts and implications for magmatic degassing. Geochim. Cosmochim. Acta 63, 729-738.

Webster, J.D., De Vivo, B., 2002. Experimental and modeled solubilities of chlorine in aluminosilicate melts, consequences of magma evolution and implications for exsolution of hydrous chloride melt at Mt. Somma-Vesuvius. Am. Mineral. 87, 1046-1061.

Webster, J.D., Sintoni, M.F., De Vivo, B., 2009-this issue. The partitioning behavior of Cl, S, and H_2O in aqueous vapor- ± saline-liquid saturated phonolitic and trachytic melts at 200 MPa. Chem. Geol. (in press).

Wyllie, P.J., Tuttle, O.F., 1961. Experimental investigation of silicate systems containing two volatile components. Am. J. Sci. 259, 128-143.

Zimova, M., Webb, S.L., 2007. The combined effects of chlorine and fluorine on the viscosity of aluminosilicate melts. Geochim. Cosmochim. Acta 71, 1553-1562.

Figure Captions:

Fig. 1: Secondary electron image of experimental glasses, on the left is one at 1 MPa (Cl-McG6) and on the right is another at 25 MPa (R30). All the experimental glasses contained no more than 10 volume percent bubbles.

Fig. 2: Cl concentration in final glasses at 1 MPa versus experimental duration. Cl concentration appears unaffected by the duration of these experiments (see text).

Fig. 3: Cl concentration in the fluid (recalculated by mass balance) versus Cl concentration in the final melt (measured by electron microprobe analysis). Distribution coefficients ($D_{Cl}^{f/m}$) are derived by the regression line fit to the data up to a maximum Cl concentration of 0.4 wt.% in the melt (see text).
A) experiments with H_2O and Cl; *B*) experiments with H_2O, Cl and CO_2.

Fig. 4: Comparison of the alkali concentration by mass balance vs. the final alkali concentrations in the melt, expressed in moles. a) K; b) Na. The samples falling in the positive region represent the fluids enriched in Na and K, a condition consistent with brine formation. Points falling in the negative region represent those glasses that incorporated the alkalis previously added as chloride solutions.

Fig. 5: Concentrations of H_2O versus Cl in the final melts. H_2O content does not vary as Cl increases. Following Webster et al. (1999), and considering that most of our experiments were at initial Cl concentrations below brine saturation, this suggests that our experiments fall in the P-T-X region where only a hydrous vapor or fluid and melt were stable.

Fig. 6: The effect of oxygen fugacity on chlorine partitioning between the melt and the fluid. a) Experiments performed at 100 MPa; b) experiments performed at 50 MPa. f_{O2} does not exert a significant influence on Cl partitioning especially at low Cl concentrations in the melt.

Fig. 7: The effect of pressure and CO_2 on chlorine partitioning between the melt and the fluid. Comparing experiments at the same pressure, we observe an increase of the affinity of Cl for the melt in the CO_2-bearing runs vs. that in the CO_2-free runs.

Fig. 8: $D_{Cl}^{f/m}$ (by weight) vs. pressure. Grey circles: H_2O-Cl experiments at NNO; grey diamonds: H_2O-Cl experiments at $\Delta NNO \geq 2$; black circles: H_2O-Cl-CO_2 experiments at NNO; black diamond: H_2O-Cl-CO_2 experiment (R13) at $\Delta NNO \geq 2$.
H_2O-Cl experiments at NNO can be fitted with the equation reported in the diagram (see text for further discussion).

Fig. 9: Comparison of Cl concentrations in melts and coexisting fluids from this study and Stelling et al. (2008) 200 MPa and 1200 °C. Tthe fluid phase in our experiments is richer in Cl than those in Stelling et al. (2008) with similarr Cl concentrations in the melt (e.g., at 0.5 wt.% Cl in the melt, Stelling et al. find 0.59 wt.% Cl in the fluid phase, while we find 5.5 wt.%). See text for further discussion.

Fig. 10: Partition coefficients (on a weight basis) for chlorine between H_2O-Cl fluid and basaltic melt found in this study between 0.1 and 200 MPa (Table 5) and in other studies using basaltic melts at 200 MPa. The concentrations of Cl in the melts of the other studies at 200 MPa is given in the column next to the symbols. Note that most results at 200 MPa are consistent with a partition coefficient near 6, as found in this study, but that a few results display partition coefficients near 2, even though the Cl concentrations in those melt are similar to melts displaying larger partition coefficients (see text).

Fig. 11: Variation of Cl in the fluid phase with pressure (solid line), calculated following equation 3 and Cl concentrations in primitive Etnean melts (for further discussion). Vertical grey bar: range of HCl concentrations in Etna's plume, which corresponds to our model-predicted Cl concentrations at pressures between 5 and 25 MPa (horizontal grey bar).
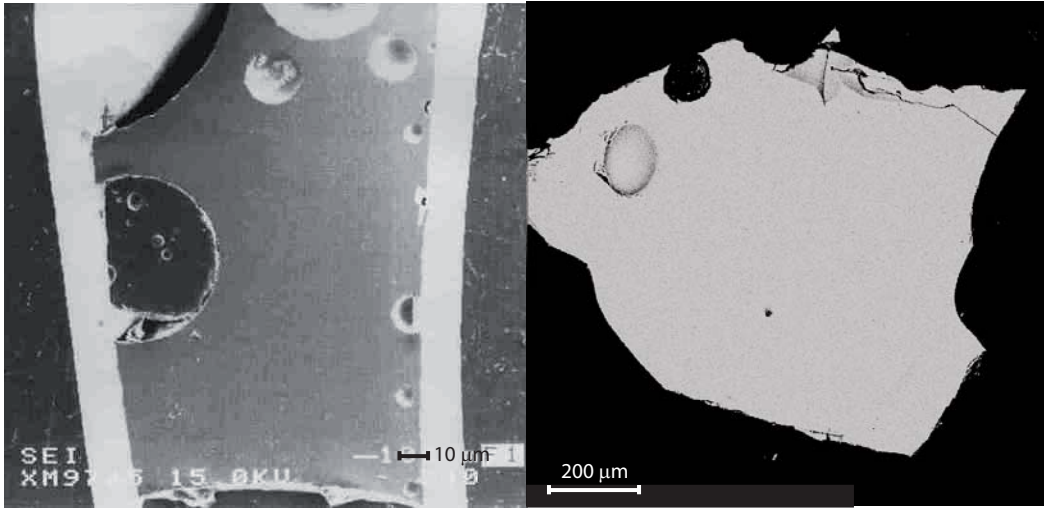
Fig. 1

Fig. 2

Fig. 3A

Fig. 3 B

Fig. 4

Fig. 5

Fig. 6

Fig. 7

Fig. 8

Fig. 9

Fig. 10
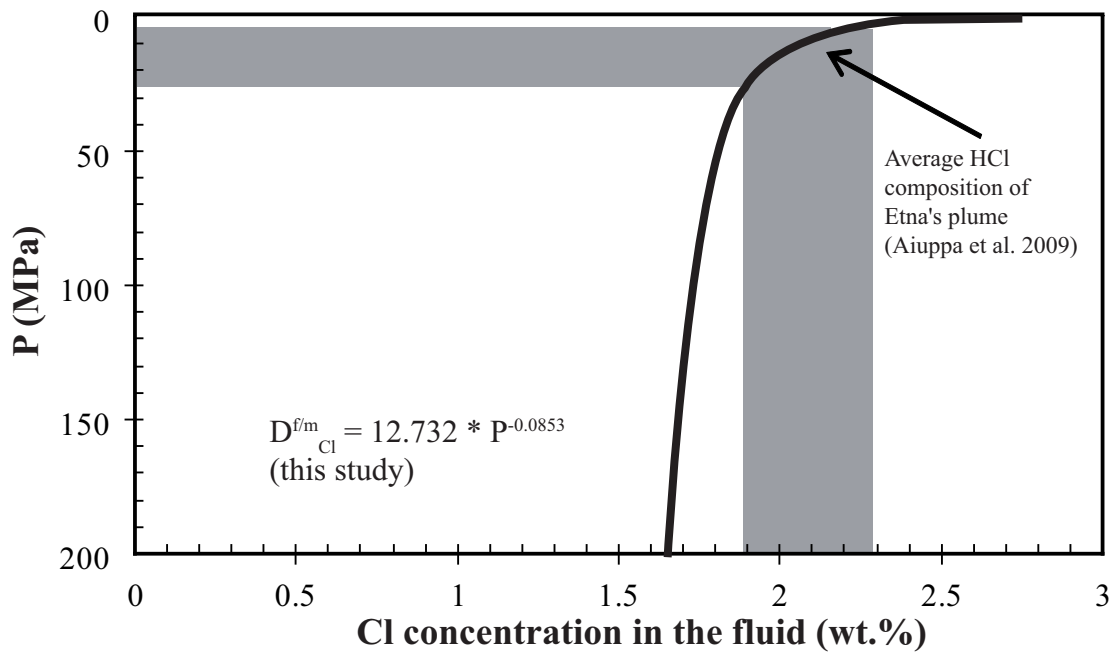
Fig. 11

Table 1: Starting material composition (Etna basalt)

wt%	*Avg* (10)	*sd*
SiO_2	47.29	0.30
TiO_2	1.70	0.11
Al_2O_3	16.21	0.17
FeO	10.86	0.24
MnO	0.17	0.09
MgO	6.76	0.13
CaO	10.73	0.27
Na_2O	3.15	0.10
K_2O	1.86	0.09
P_2O_5	0.67	0.06
Cl	0.14	<0.01
Total	99.53	

Table 2a: Experimental runs, conditions and results for CO_2-free experiments

Experiment designation	ΔNNO	P (MPa)	T (°C)	Duration (hours)	Cl charged (mg)	H_2O charged (mg)	Glass mass (mg)	Cl in glass (wt.%)[1]	Cl in fluid (wt.%)[1,2]	fl/melt initial	fl/melt run	H_2O in glass (wt.%)[1]
R5-1	+2	51	1200 ± 3	4	0.02	3.07	95.7	0.15 (00)	0.39 (02)	0.032	0.017	1.48 (08)
R5-2		51	1200 ± 3	4	0.06	3.10	93.7	0.18 (00)	1.02 (11)	0.034	0.020	1.32 (35)
R5-3		51	1200 ± 3	4	0.10	3.13	100.1	0.22 (00)	1.11 (09)	0.032	0.015	1.59 (15)
R5-4		51	1200 ± 3	4	0.20	3.16	101.3	0.31 (00)	1.15 (12)	0.033	0.015	1.58 (24)
R5-5		51	1200 ± 3	4	0.39	2.96	100.5	0.44 (02)	4.91 (30)	0.033	0.014	1.51 (06)
R5-6		51	1200 ± 3	4	0.59	2.87	100.0	0.55 (02)	10.55 (80)	0.035	0.015	1.45 (18)
R3-1	+2	105	1200 ± 3	4	0.02	4.06	102.2	0.17 (00)	1.08 (13)	0.040	0.016	2.28 (19)
R3-2		105	1200 ± 3	4	0.07	3.97	100.2	0.21 (01)	1.46 (32)	0.041	0.016	2.28 (44)
R3-3		105	1200 ± 3	4	0.13	4.08	100.0	0.25 (01)	1.97 (25)	0.043	0.016	2.42 (19)
R3-4		105	1200 ± 3	4	0.26	4.06	98.0	0.30 (01)	6.43 (72)	0.046	0.017	2.37 (18)
R3-5		105	1200 ± 3	4	0.51	3.87	100.3	0.54 (02)	7.38 (76)	0.047	0.014	2.41 (05)
R3-6		105	1200 ± 3	4	0.75	3.70	100.8	0.77 (02)	6.89 (86)	0.049	0.018	1.93 (29)
R9-3		106	1200 ± 3	4	1.07	3.85	101.6	0.87 (01)	22.86 (2.93)	0.054	0.012	2.62 (22)
R9-1		106	1200 ± 3	4	2.21	4.00	110.1	1.07 (01)	48.61 (7.53)	0.072	0.020	2.39 (21)
R9-2		106	1200 ± 3	4	1.98	0.00	97.8	1.64 (02)	0.00	n.a.	n.a.	0.65 (05)
Cl-McG1*	-0.3	1	1260 ± 5	12	0.01	0.53	11.9	0.16 (01)	0.60 (08)	0.045	0.043	0.14 (00)
Cl-McG2*		1	1260 ± 5	12	0.04	0.77	12.3	0.34 (04)	1.69 (24)	0.066	0.062	0.15 (00)
Cl-McG3*		1	1260 ± 5	2	0.04	0.68	12.1	0.31 (06)	1.81 (01)	0.059	0.055	0.13 (00)
Cl-McG4**		1	1260 ± 5	12	0.04	0.34	13.3	0.27 (01)	2.63 (04)	n.a.	0.025	0.14 (00)
Cl-McG5**		1	1260 ± 5	2	0.04	0.31	12.3	0.25 (01)	3.61 (04)	n.a.	0.025	0.13 (01)
Cl-McG6**		1	1260 ± 5	2	0.09	0.43	11.7	0.47 (00)	7.52 (08)	n.a.	0.039	0.16 (01)
Cl-McG7*		1	1260 ± 5	12	0.24	0.54	14.1	1.31 (02)	10.86 (06)	0.055	0.040	0.15 (00)
Cl-McG8*		1	1260 ± 5	12	0.34	0.55	14.2	1.34 (01)	23.18 (11)	0.063	0.046	0.15 (00)
R30-1	+0.24	26	1200 ± 3	3	0.01	1.29	53.2	0.13 (00)	1.01 (03)	0.024	0.013	1.11 (08)
R30-3		26	1200 ± 3	3	0.04	1.23	53.8	0.17 (00)	2.34 (09)	0.024	0.011	1.15 (16)
R30-4		26	1200 ± 3	3	0.09	1.37	54.8	0.24 (00)	3.83 (19)	0.027	0.012	1.29 (23)
R30-5		26	1200 ± 3	3	0.16	1.23	55.1	0.34 (00)	10.14 (1.29)	0.027	0.007	1.47 (35)
R30-6		26	1200 ± 3	3	0.26	1.29	51.7	0.40 (01)	15.87 (40)	0.033	0.014	1.24 (09)
R22-1	+0.77	47	1200 ± 3	3	0.01	2.47	69.7	0.14 (00)	0.78 (05)	0.036	0.018	1.71 (19)
R22-2		47	1200 ± 3	3	0.04	2.42	70.2	0.18 (00)	0.88 (05)	0.036	0.015	1.86 (06)
R22-3		47	1200 ± 3	3	0.08	2.47	69.9	0.21 (01)	1.91 (11)	0.037	0.016	1.88 (07)
R22-4		47	1200 ± 3	3	0.16	2.46	70.4	0.29 (01)	3.90 (26)	0.038	0.015	2.02 (14)
R22-5		47	1200 ± 3	3	0.32	2.38	70.4	0.42 (01)	11.39 (77)	0.041	0.013	2.10 (13)
R22-6		47	1200 ± 3	3	0.61	2.16	71.4	0.78 (01)	15.22 (89)	0.043	0.012	1.91 (09)
R14-1	+0.36	102	1200 ± 3	3	0.02	3.17	72.1	0.17 (01)	0.00 (00)	0.044	0.009	3.37 (27)
R14-2		102	1200 ± 3	3	0.06	3.10	69.6	0.21 (01)	0.11 (02)	0.045	0.009	3.41 (12)
R14-3		102	1200 ± 3	3	0.10	3.32	81.6	0.25 (01)	1.02 (30)	0.042	0.005	3.41 (16)
R14-4		102	1200 ± 3	3	0.22	3.56	79.5	0.35 (03)	5.47 (95)	0.048	0.010	3.34 (17)
R14-5		102	1200 ± 3	3	0.46	3.45	83.9	0.57 (01)	12.89 (3.11)	0.047	0.006	3.37 (06)
R14-6		102	1200 ± 3	3	0.70	3.40	80.9	0.80 (01)	32.31(10.40)	0.051	0.005	3.66 (13)
R14-7		102	1200 ± 3	3	0.91	3.29	79.0	0.99 (01)	25.78 (3.71)	0.053	0.009	3.26 (06)
R14-8		102	1200 ± 3	3	2.51	3.60	80.4	1.94 (05)	74.75 (16.82)	0.076	0.015	3.82 (44)
R33-0	+0.3	101	1200 ± 3	3	0.00	4.20	65.1	0.13 (00)	0.17 (02)	0.065	0.027	3.59 (11)
R33-1		101	1200 ± 3	3	0.06	3.04	64.1	0.21 (00)	0.65 (12)	0.048	0.008	3.79 (12)
R33-3		101	1200 ± 3	3	0.18	3.22	66.2	0.36 (01)	4.83 (1.05)	0.051	0.008	3.86 (22)
R33-5		101	1204 ± 3	3	0.75	3.95	66.3	1.00 (01)	11.25 (1.48)	0.071	0.018	4.05 (12)
R34-0		202	1200 ± 3	3	0.00	4.20	60.6	0.18 (00)	0.00 (00)	0.069	0.009	5.66 (58)
R34-1		202	1200 ± 3	3	0.08	4.42	65.3	0.28 (01)	2.34 (87)	0.069	0.003	6.04 (06)
R34-3		202	1200 ± 3	3	0.26	4.64	64.6	0.52 (01)	5.49 (1.97)	0.076	0.006	6.11 (13)
R34-5		202	1200 ± 3	3	1.03	5.47	65.9	1.46 (06)	8.13 (1.54)	0.099	0.026	5.35 (29)

* Cl - in experiments

** Cl - out experiments

[1] Errors are 1σ

[2] Cl in fluid (wt%): concentration of Cl in the fluid phase, calculated through mass balance (see text)

Table 2b: Experimental runs, conditions and results for CO_2-bearing experiments

Experiment designation	ΔNNO	P (MPa)	T (°C)	Duration (hours)	Cl charged (mg)	H_2O charged (mg)	Glass mass (mg)	Cl in glass (mg)[1]	Cl in fluid (wt.%)[1,2]	fl/melt initial	fl/melt run	H_2O in glass (wt.%)[1]	CO_2 in glass (ppm)[1]	CO_2 in fluid[3] (wt.%)
R13-1	+1.7	101	1200 ± 3	4	0.02	3.17	79.8	0.18 (00)	0.16 (02)	0.051	0.027	2.22 (15)	358 (26)	37
R13-2		101	1200 ± 3	4	0.06	3.29	77.7	0.21 (00)	1.05 (13)	0.053	0.027	2.36 (12)	414 (81)	33
R13-3		101	1200 ± 3	4	0.10	3.32	78.0	0.22 (00)	2.22 (28)	0.057	0.031	2.22 (17)	282 (12)	36
R13-4		101	1200 ± 3	4	0.21	3.28	78.8	0.32 (01)	3.74 (52)	0.055	0.027	2.39 (19)	401 (1)	34
R13-5		101	1200 ± 3	4	0.42	3.21	80.4	0.40 (01)	9.88 (2.10)	0.060	0.028	2.39 (36)	351 (12)	37
R13-7		101	1200 ± 3	4	0.86	3.08	80.4	0.78 (01)	13.28 (1.29)	0.066	0.031	2.12 (11)	319 (7)	35
R13-8		101	1200 ± 3	4	2.16	4.00	80.6	1.63 (02)	24.33 (1.99)	0.107	0.050	2.31 (16)	377 (25)	21
R31-1	+0.03	26	1200 ± 3	3	0.01	1.29	51.6	0.14 (00)	0.63 (03)	0.031	0.017	1.38 (03)	66[4]	36
R31-3		26	1200 ± 3	3	0.04	1.23	52.6	0.18 (00)	1.34 (07)	0.032	0.017	1.30 (07)	82[4]	40
R31-4		26	1200 ± 3	3	0.07	1.19	54.4	0.23 (00)	2.18 (27)	0.031	0.014	1.46 (19)	47[4]	50
R31-5		26	1200 ± 3	3	0.16	1.23	54.2	0.36 (00)	4.94 (31)	0.032	0.012	1.54 (05)	24[4]	39
R31-6		26	1200 ± 3	3	0.25	1.21	53.9	0.46 (00)	8.25 (39)	0.035	0.014	1.38 (05)	65[4]	36
R19-1	+0.5	48	1200 ± 3	3	0.01	2.47	67.8	0.20 (00)	0.37 (04)	0.051	0.028	2.09 (06)	297 (65)	42
R19-2		48	1200 ± 3	3	0.05	2.52	66.6	0.24 (00)	0.75 (05)	0.049	0.030	1.69 (09)	176 (23)	31
R19-3		48	1200 ± 3	3	0.08	2.56	67.8	0.28 (01)	0.77 (09)	0.051	0.027	2.04 (18)	245 (57)	38
R19-4		48	1200 ± 3	3	0.17	2.64	67.6	0.38 (02)	1.55 (13)	0.054	0.029	2.00 (02)	286 (60)	36
R19-6		48	1200 ± 3	3	0.48	2.34	67.0	0.74 (01)	5.03 (41)	0.058	0.027	1.88 (05)	189 (45)	40
R19-7		48	1200 ± 3	3	0.66	2.38	66.5	0.86 (02)	10.11 (89)	0.063	0.028	2.06 (08)	343 (50)	40
R17-1	+0.29	100	1200 ± 3	3	0.02	3.66	78.8	0.17 (01)	0.40 (07)	0.057	0.028	2.73 (17)	349 (9)	35
R17-2		100	1200 ± 3	3	0.07	3.68	72.9	0.20 (00)	1.51 (24)	0.063	0.029	3.09 (03)	297 (65)	39
R17-3		100	1200 ± 3	3	0.11	3.61	71.3	0.22 (01)	2.67 (49)	0.065	0.027	3.29 (03)	325 (49)	42
R17-5		100	1200 ± 3	3	0.43	3.29	74.5	0.57 (05)	5.96 (1.84)	0.065	0.019	3.42 (15)	349 (41)	58
R17-7		100	1200 ± 3	3	1.01	3.64	75.8	1.09 (03)	10.39 (1.75)	0.079	0.027	3.11 (10)	389 (99)	40
R17-8		100	1200 ± 3	3	2.88	4.20	78.5	1.77 (02)	38.74 (3.70)	0.130	0.057	3.21 (17)	336 (23)	23

[1] Errors are ±1σ.

[2] Cl in fluid (wt%): concentration of Cl in the fluid phase, calculated through mass balance (see text).

[3] Concentration of CO_2 computed for the fluid phase.

[4] Computed concentration of CO_2 in the melt following Lesne (2008) (see text).

Table 3: Major elements analysis of all Cl-experiments

Run#	SiO2 (wt%)	TiO2 (wt%)	Al2O3 (wt%)	FeO (wt%)	MnO (wt%)	MgO (wt%)	CaO (wt%)	Na2O (wt%)	K2O (wt%)	P2O5	Cl	Total
R5-1	46.12	1.57	15.94	9.35	0.17	6.52	10.03	3.54	1.86	n.a.	0.15	95.24
R5-2	46.28	1.62	15.88	9.25	0.12	6.40	9.94	3.42	1.82	n.a.	0.18	94.90
R5-3	46.66	1.62	16.22	9.12	0.20	6.41	10.04	3.49	1.86	n.a.	0.22	95.83
R5-4	46.06	1.60	16.08	9.31	0.17	6.35	9.98	3.71	1.98	n.a.	0.31	95.55
R5-5	46.70	1.59	16.19	9.13	0.11	6.30	9.75	3.60	1.98	n.a.	0.45	95.78
R5-6	46.38	1.61	16.10	9.01	0.15	6.30	9.93	3.78	1.98	n.a.	0.55	95.80
R3-1	45.16	1.56	15.74	9.91	0.19	6.40	9.88	3.26	1.79	n.a.	0.17	94.06
R3-2	45.46	1.55	16.01	9.27	0.14	6.33	9.74	3.23	1.84	n.a.	0.21	93.77
R3-3	45.38	1.55	15.89	9.56	0.13	6.34	9.90	3.29	1.81	n.a.	0.25	94.10
R3-4	45.12	1.53	15.70	9.54	0.16	6.32	9.72	3.67	1.97	n.a.	0.30	94.01
R3-5	45.11	1.53	15.69	9.48	0.18	6.25	9.73	3.44	1.90	n.a.	0.54	93.87
R3-6	45.27	1.57	16.04	9.63	0.11	6.31	9.84	3.24	1.81	n.a.	0.77	94.60
R9-3	44.94	1.63	15.07	9.60	0.20	6.30	10.07	3.73	2.11	n.a.	0.87	94.52
R9-1	44.15	1.58	14.85	9.26	0.15	6.19	9.88	4.38	2.34	n.a.	1.07	93.84
R9-2	46.32	1.64	15.67	9.41	0.14	6.44	10.24	4.19	2.52	n.a.	1.64	98.21
Cl-McG1*	47.21	1.68	16.59	9.99	0.18	6.01	10.60	3.21	1.87	0.53	0.16	98.02
Cl-McG2*	46.80	1.68	16.58	9.97	0.18	6.03	10.64	3.34	1.83	0.53	0.34	97.91
Cl-McG3*	47.47	1.64	16.52	9.59	0.18	5.83	10.69	3.56	1.81	0.51	0.31	98.11
Cl-McG4**	47.57	1.69	16.54	9.77	0.18	5.95	10.62	3.70	1.84	0.54	0.27	98.68
Cl-McG5**	47.17	1.67	16.53	10.05	0.18	5.90	10.17	3.47	1.90	0.57	0.25	97.86
Cl-McG6**	47.27	1.69	16.52	9.08	0.16	5.92	10.93	3.79	1.71	0.54	0.47	98.09
Cl-McG7*	46.06	1.65	16.10	10.02	0.16	5.80	10.36	4.91	1.66	0.50	1.31	98.55
Cl-McG8*	46.02	1.63	16.12	10.05	0.17	5.80	10.27	5.20	1.53	0.51	1.34	98.64
R30-1	46.95	1.67	15.73	8.99	0.16	6.51	10.26	3.24	1.88	0.62	0.13	96.14
R30-3	46.90	1.65	15.72	9.02	0.15	6.49	10.16	3.22	1.93	0.66	0.17	96.07
R30-4	47.06	1.62	15.77	8.98	0.16	6.41	9.98	3.31	1.92	0.64	0.24	96.09
R30-5	46.57	1.65	15.66	9.02	0.17	6.54	10.20	3.32	1.93	0.64	0.34	96.05
R30-6	46.61	1.64	15.54	8.98	0.21	6.56	10.24	3.40	1.91	0.62	0.40	96.11
R22-1	45.48	1.61	15.33	9.73	0.16	6.46	10.27	3.00	1.75	n.a.	0.14	93.94
R22-2	46.22	1.61	15.62	9.25	0.14	6.32	10.15	3.14	1.94	n.a.	0.18	94.58
R22-3	45.51	1.64	15.36	9.32	0.11	6.34	10.15	3.11	1.85	n.a.	0.21	93.60
R22-4	45.43	1.63	15.37	9.31	0.22	6.38	10.11	3.17	1.93	n.a.	0.29	93.84
R22-5	45.25	1.59	15.22	9.03	0.17	6.34	10.16	3.26	1.95	n.a.	0.42	93.38
R22-6	44.65	1.56	15.21	9.13	0.16	6.35	10.11	3.40	2.11	n.a.	0.78	93.45
R14-1	46.58	1.65	15.43	9.25	0.22	6.54	10.28	3.26	1.84	n.a.	0.17	95.21
R14-2	46.39	1.65	15.33	9.22	0.17	6.61	10.30	3.29	1.80	n.a.	0.21	94.97
R14-3	46.49	1.67	15.38	9.21	0.18	6.44	10.13	3.34	1.81	n.a.	0.25	94.91
R14-4	45.21	1.62	14.86	9.12	0.13	6.43	10.08	3.40	1.83	n.a.	0.35	93.02

Table 3 (continued)

Run#	SiO2 (wt%)	TiO2 (wt%)	Al2O3 (wt%)	FeO (wt%)	MnO (wt%)	MgO (wt%)	CaO (wt%)	Na2O (wt%)	K2O (wt%)	P2O5	Cl	Total
R14-5	44.71	1.59	14.74	8.61	0.15	6.34	9.86	4.45	2.59	n.a.	0.57	93.60
R14-6	45.40	1.57	15.06	8.76	0.16	6.51	10.09	3.88	1.89	n.a.	0.80	94.13
R14-7	45.64	1.63	15.10	8.92	0.22	6.48	10.14	3.73	2.02	n.a.	0.99	94.88
R14-8	46.22	1.64	15.26	8.95	0.20	6.46	10.06	3.52	1.99	n.a.	1.94	96.23
R33-0	45.94	1.63	15.69	8.99	0.15	6.48	10.07	3.18	1.73	0.67	0.13	94.67
R33-1	46.11	1.63	15.63	9.05	0.15	6.39	9.83	3.20	1.83	0.66	0.21	94.70
R33-3	45.83	1.62	15.71	9.00	0.14	6.39	9.92	3.37	1.88	0.66	0.36	94.87
R33-5	44.98	1.63	15.35	8.68	0.14	6.36	9.64	3.85	2.11	0.66	1.00	94.40
R34-0	45.29	1.60	15.59	8.75	0.17	6.44	9.86	3.08	1.71	0.67	0.18	93.32
R34-1	44.85	1.61	15.30	8.59	0.10	6.30	9.56	3.11	1.72	0.66	0.28	92.09
R34-3	44.63	1.60	15.33	8.59	0.17	6.18	9.69	3.37	1.84	0.64	0.52	92.56
E34-5	43.43	1.52	14.77	8.35	0.18	6.06	9.49	3.69	2.18	0.67	1.41	91.80
R13-1	44.52	1.69	15.45	9.60	0.23	6.44	10.34	3.09	1.83	n.a.	0.18	93.37
R13-2	44.05	1.68	15.58	9.61	0.15	6.46	10.29	3.16	1.84	n.a.	0.21	93.04
R13-3	43.20	1.68	15.38	9.77	0.16	6.40	10.21	3.13	1.83	n.a.	0.22	91.98
R13-4	42.89	1.65	15.19	9.49	0.14	6.39	10.12	3.19	1.88	n.a.	0.32	91.25
R13-5	43.10	1.62	15.22	9.70	0.15	6.43	10.13	3.24	1.94	n.a.	0.40	91.94
R13-7	44.43	1.64	15.13	9.46	0.14	6.33	10.04	3.53	2.15	n.a.	0.78	93.64
R13-8	43.83	1.59	14.86	9.09	0.17	6.21	9.68	4.25	2.44	n.a.	1.63	93.76
R31-1	47.03	1.67	15.74	8.96	0.16	6.55	10.23	3.18	1.84	0.65	0.14	96.15
R31-3	46.62	1.62	15.69	8.94	0.17	6.61	10.30	3.25	1.86	0.62	0.18	95.86
R31-4	46.68	1.68	15.66	8.93	0.12	6.56	10.31	3.24	1.88	0.64	0.23	95.95
R31-5	46.68	1.68	15.59	9.04	0.14	6.51	10.23	3.37	2.01	0.62	0.36	96.24
R31-6	46.53	1.65	15.71	8.97	0.17	6.54	10.34	3.41	1.97	0.63	0.46	96.38
R19-1	47.01	1.69	15.60	9.35	0.17	6.50	10.18	3.31	1.82	n.a.	0.20	95.84
R19-2	46.99	1.63	15.44	9.44	0.17	6.44	10.19	3.40	1.81	n.a.	0.24	95.75
R19-3	47.02	1.65	15.54	9.44	0.14	6.54	10.18	3.50	1.81	n.a.	0.28	96.12
R19-4	47.18	1.67	15.61	9.24	0.14	6.42	10.00	3.56	1.94	n.a.	0.38	96.14
R19-6	46.71	1.61	15.45	9.41	0.18	6.48	10.06	3.82	2.03	n.a.	0.74	96.50
R19-7	46.63	1.58	15.26	9.10	0.16	6.35	10.01	3.86	2.11	n.a.	0.86	95.92
R17-1	46.57	1.65	15.50	9.04	0.14	6.47	10.09	3.34	1.84	n.a.	0.17	94.80
R17-2	46.55	1.60	15.41	8.76	0.14	6.41	10.23	3.36	1.85	n.a.	0.20	94.50
R17-3	46.61	1.56	15.32	8.71	0.27	6.40	9.96	3.33	1.88	n.a.	0.22	94.26
R17-5	46.24	1.62	15.41	8.69	0.13	6.34	10.00	3.66	1.96	n.a.	0.57	94.62
R17-7	46.08	1.58	15.03	8.38	0.16	6.30	9.88	3.95	2.23	n.a.	1.10	94.68
R17-8	44.37	1.50	14.69	7.65	0.13	6.18	9.43	4.96	2.47	n.a.	1.77	93.15

Table 4a: oxygen fugacity determination for H_2O-Cl experiments

RUN#	P_{H2} (MPa)	P_{tot} (MPa)	γH_2O^*	γH_2^*	$\log f_{O2}$ @NNO	$\log f_{O2}$ sample	ΔNNO sample
14	0.35	100	1	1.10	-7.69	-7.33	+0.36
22	0.13	50	1	1.07	-7.70	-6.93	+0.77
30	0.11	25	1	1.03	-7.71	-7.47	+0.24

Table 4b: oxygen fugacity determination for H_2O-Cl-CO_2 experiments

RUN#	P_{H2} (MPa)	P_{tot} (MPa)	$CO_2^{initial}$ (wt%)	$H_2O^{initial}$ (wt%)	X_{H2O}^{gas} (mol)	X_{CO2}^{gas} (mol)	f_{H2O} (MPa)	f_{CO2} (MPa)	γH_2^*	$\log f_{O2}$ sample	$\log f_{O2}$ @NNO	ΔNNO sample
17	0.35	100	1.2	4.0	0.72	0.275	68.2	38.9	1.05	-7.62	-7.69	+0.07
19	0.13	50	1.0	3.5	0.63	0.370	38.2	12.5	1.03	-7.20	-7.70	+0.50
31	0.11	25	0.5	2.0	0.64	0.360	19.1	6.1	1.00	-7.68	-7.71	+0.03

[*]after Belonoshko et al., 1992.

Table 5: Partition coefficients at different pressures

	P (MPa)	$D^{f/m}_{Cl}$ [1]	Kd [2]
H$_2$O-Cl, ~ NNO	1	10.8	2.9
	25	13.9	3.5
	50	9.8	2.3
	100	9.0	1.7
	200	5.9	1.3
H$_2$O-Cl, NNO $\geq$ 2	50	4.2	1.2
	100	13.0	3.1
H$_2$O-Cl-CO$_2$, ~ NNO	25	7.9	2.8
	50	3.3	1.1
	100	8.3	2.9
H$_2$O-Cl-CO$_2$, NNO $\geq$ 2	100	5.8	2.5

[1] wt.%-based partition coefficient
[2] Mole fraction-based partition coefficient